

# Exploring Novel Quantum Criticality in Strained Graphene

S. Arya<sup>1,\*</sup>, M. S. Laad<sup>1,†</sup> and S. R. Hassan<sup>1‡</sup>

<sup>1</sup>*Institute of Mathematical Sciences (Homí Bhabha National Institute), Taramani, Chennai 600113, India*

Strain tuning is increasingly being recognized as a clean tuning parameter to induce novel behavior in quantum matter. Motivated by the possibility of straining graphene up to 20 percent, we investigate novel quantum criticality due to interplay between strain-induced anisotropic band structure and critical antiferromagnetic spin fluctuations (AFSF) in this setting. We detail how this interplay drives (i) a quantum phase transition (QPT) between the Dirac-semimetal-incoherent pseudogapped metal-correlated insulator as a function of strain ( $\epsilon$ ), and (ii) critical AFSF-driven divergent nematic susceptibility near critical strain ( $\epsilon_c$ ) manifesting as critical singularities in magneto-thermal expansion and Grüneisen co-efficients. The correlated band insulator at large strain affords realization of a two-dimensional dimerized spin-singlet state due to this interplay, and we argue how doping such an insulator can lead to a spin-charge separated metal, leading to anomalous metallicity and possible unconventional superconductivity. On a wider front, our work serves to illustrate the range of novel states realizable by strain-tuning quantum materials.

PACS numbers: 25.40.Fq, 71.10.Hf, 74.70.-b, 63.20.Dj, 63.20.Ls, 74.72.-h, 74.25.Ha, 76.60.-k, 74.20.Rp

The exciting discovery of single-layer graphene has spawned a tremendous burst of activity<sup>1</sup> on fundamental and applied grounds. It is the strongest electronic material, capable of sustaining reversible elastic deformations in excess of 20 percent.<sup>2</sup> Besides, graphene possesses rich electronic properties, originating from gapless, linearly dispersing Dirac-like excitations<sup>3</sup>. Attractive features like high mobility, absence of backscattering and strong field effects hold out the promise for future devices, but such possibilities are hindered by the gapless spectrum. Inducement of a gap by quantum confinement is possible, but this also gives rise to edge roughness, with deleterious effect on electronic properties.

Recently, strain engineering has been studied<sup>4</sup> as a way to profitably unite seemingly independent mechanical and electronic properties of graphene. Experimental studies indicate that reversible and controlled strain up to 20 percent can be produced in graphene<sup>5</sup>, opening a unique opportunity to realize this aspect. While detailed investigation of this interplay within one-electron band structure has been carried out<sup>4</sup>, possibility of novel physics arising due to interplay between strain-modified electronic structure and electron-electron interactions has not received much attention. Observed breakdown of the Wiedemann-Franz law<sup>6</sup> near the charge neutrality point betrays the effect of sizable  $e - e$  interactions in graphene. In this light, one may anticipate that a strain-modified band structure could give rise to novel quantum phase transition(s) and novel physical responses as a result of interplay between an anisotropic electronic structure and local Coulomb interactions. In this letter, we explore the possibility of inducing novel quantum phase transitions in (20 percent) strained graphene as a consequence of interplay between strong antiferromagnetic spin fluctuations (AFSF) and anisotropic band structure under strain. We stress that our analysis has potentially wider consequences for materials with honeycomb lattice structures, but with correlations not so strong as to induce a Mott transition (which requires complementary

DMFT-like analyses<sup>7</sup>).

Our starting point is the electronic structure of graphene under strain<sup>4</sup>. We have repeated their earlier analysis. As shown in detail in Supplementary Information (SI)<sup>8</sup> and in Fig. 1, zig-zag strain induces sizable reconstruction of the electronic structure: it moves the Dirac point away from  $K$  toward  $M$  for finite strain, and (ii) beyond a critical zig-zag strain ( $\epsilon_c \approx 0.23$ ), a band-insulating gap develops in graphene and the “Dirac point” gets shifted to the  $M$  point. In contrast, arm-chair strain has very little effect on the electronic structure, so we will restrict ourselves to zig-zag strain hereafter. Though scarcely studied<sup>9,10</sup>,  $e - e$  interactions

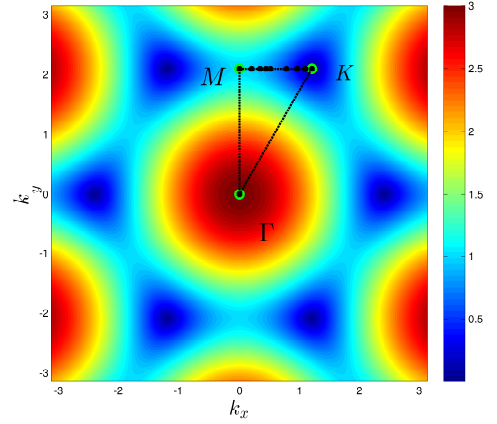


FIG. 1. Contour plot of the valence band for the unstrained case. As the strain is increased, the Dirac point shifts from the  $K$  point to the  $M$  point.

are not negligible in graphene. Realistic estimates put the intra-orbital Hubbard  $U = U_{pp} \simeq 8 - 10$  eV within first-principles studies. Our strategy is to vary  $U/t$  from small to realistic values, where  $t$  is the tight-binding hopping integral between nearest-neighbor  $p_z$  orbitals

on the honeycomb lattice. Under zig-zag strain, the zig-zag hoppings  $t_{x,x} = t_{y,y}$  progressively reduce, while the  $z - z$  hopping  $t_{z,z}$  increases. Thus, interplay with Hubbard correlations is, very generally, expected to (i) enhance strain-induced anisotropy, (ii) produce a tendency to Mott localization beyond a critical  $U_c/t$ , and (iii) perhaps most importantly, to induce exotic semi-metallic/insulating states around critical strain  $\epsilon = \epsilon_c$  when  $U$  is varied across a critical  $U_c$ . In the  $D = 2$  case that applies in graphene, long-range AFSF should be very relevant. While dynamic-mean-field theory (DMFT)<sup>7</sup> or its cluster extensions can reveal “Mottness” effects, they cannot, by construction, access the effects of long-ranged critical AFSF and possible AF quantum criticality at low  $T$ .

Here, we investigate the role of long-range critical AFSF in strained graphene. We employ the Two-Particle Self-Consistent (TPSC) theory: TPSC exploits the Pauli principle and exact sum rules<sup>11</sup> relating wave-vector dependent susceptibilities to *local* correlators to formulate a non-trivially renormalized version of the random-phase approximation (RPA). It is similar in spirit to the self-consistent renormalization (SCR) theory of Moriya and co-workers<sup>12</sup>. Use of the renormalized Hubbard  $U$  (different for charge and spin channels),  $U_{sp} = U \langle n_{\uparrow} n_{\downarrow} \rangle / \langle n_{\uparrow} \rangle \langle n_{\downarrow} \rangle$  leads to a negative feedback in RPA, preventing the divergence of the spin susceptibility at *any* finite  $T$ , in accord with stringent Mermin-Wagner restrictions in  $D = 2$ . Further, TPSC also recovers quantum critical (QC)-“renormalized classical (RC)” and QC-quantum disordered (QD) crossovers at low but finite  $T$ , and yields low- $T$  AF correlation lengths in good accord with non-linear sigma model (NLSM) predictions<sup>13</sup>. It is thus an excellent approximation for  $D = 2$  when coupling of carriers to long-range magnetic fluctuations is dominant. Indeed, TPSC has been extensively employed<sup>14,15</sup> within the itinerant spin-fluctuation theory to study AF quantum criticality in magnetic metals within the framework of Hubbard models.

We now present our results for strained graphene, relegating technical details to SI<sup>8</sup>. For each value of strain ( $\epsilon$ ), we vary the Hubbard  $U$  in the interval  $0 < U < 3.5$  eV choosing an unstrained value of  $t = 1.0$  eV. In Fig. 2, we show the imaginary part of the self-energy,  $\text{Im}\Sigma(i\omega_n)$ <sup>8</sup> at the strain shifted “Dirac” point as a function of Matsubara frequency  $i\omega_n$ . For zero or small ( $\epsilon = 0.05$ ) strain, the Dirac LFL metal remains stable for the range of  $U/t$  we consider, as seen by the fact that  $-\text{Im}\Sigma(i\omega_n) = A(i\omega_n)$  for small  $U$ <sup>8</sup>. For  $0.1 < \epsilon < 0.23$ , however, we find  $\text{Im}\Sigma(i\omega_n) = A(\epsilon)i\omega_n$ , implying correlated Landau Fermi liquid (LFL), or Dirac liquid metallicity, for  $U < U_c(\epsilon)$ .<sup>8</sup> However, for larger  $\epsilon$ -dependent  $U > U_c(\epsilon)$ ,  $\text{Im}\Sigma(i\omega_n)$  shows anomalous behavior:  $-\text{Im}\Sigma(i\omega_n)$  *increases* as  $\omega_n \rightarrow 0$ , reflecting appearance of a *pseudogap* in the one-particle excitation spectrum. In the inset, we show how  $A(\epsilon)$  develops an anomaly around  $U_c/t = 3.5$ . Further, since gapless electronic states exist only at the “Dirac” point,  $\text{Im}\Sigma(\omega_n)$  also re-

flects the  $T$ -dependence of the *dc* resistivity: thus, given  $\rho_{dc}(T) = AT^2$  in the LFL regime, we expect the A-co-efficient of the resistivity to show a similar anomaly, reflecting a change from LFL metal to an incoherent non-LFL metal as  $U \rightarrow U_c$  around the critical strain. Within TPSC, the origin of this feature is associated with

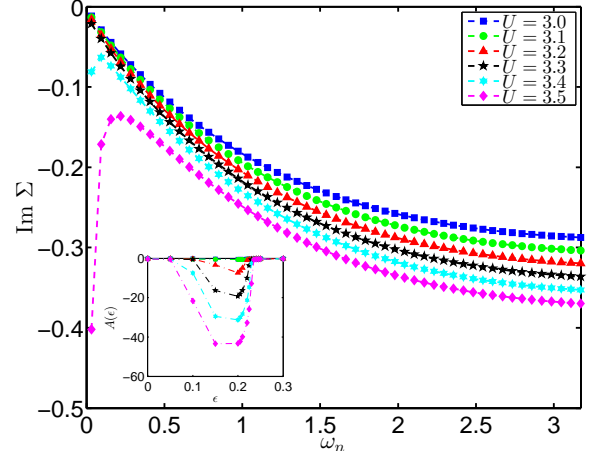


FIG. 2. Imaginary part of the self-energy  $\Sigma$  as a function of Matsubara frequency  $\omega_n$ , for  $\epsilon = 0.23$ . The inset shows how the  $A(\epsilon)$  co-efficient of  $-\text{Im}\Sigma(\omega_n)$  develops clear anomaly around  $U/t = 3.4$ .

the coupling of itinerant  $p_z$ -band carriers to long-ranged, critical AF spin fluctuations (AFSF). In Fig. 3, we show that while the AF correlation length ( $\xi_{afm}$ ) is finite for  $U < U_c$ , it indeed diverges (for low  $T$ ,  $\beta = 1/T = 200$ ) at  $T \rightarrow 0$  for  $U \geq U_c$ , confirming this view. It is known that  $\xi_{afm} \simeq e^{a(U)/T}$  in the quantum critical region within TPSC (see Fig. 3), in accord with predictions of the NLSM approach. These features are thus manifestations of the crossover from QD to the QC regime of AFSF as  $U$  increases: it is the coupling of itinerant  $p_z$  carriers (encoded in the bare one-electron propagator,  $G_0(\mathbf{k}, i\omega_n)$ ) to nearly critical AFSF, encoded in the spin susceptibility  $\chi_s(\mathbf{q}, i\omega_n) \simeq [i\omega_n + q + \xi^{-1}(T)]^{-1}$  with  $\xi_{afm}(T)$  as above that drives the QD-QC crossover. As expected, in Fig. 3, we show that increasing strain (toward  $\epsilon_c$ ) reduces  $U_c$  for the QD-QC crossover. This is due to the fact that reduction in  $t_{x,x}$  along the zig-zag direction under strain enhances the effective  $U/t$  anisotropically (it becomes larger for the zig-zag relative to  $z - z$  bonds), resulting in enhanced AFSF for smaller  $U/t_{x,x}$ . This also implies that the renormalized AFSF under strain will be enhanced by nearly-divergent  $\chi_s(\mathbf{q}, i\omega_n)$ , and that the feedback effect of the anisotropic AFSF will in turn enhance the electronic anisotropy. While this issue requires a self-consistent extension of TPSC in its current form, we consider this issue (see below) while investigating strain-enhanced nematicity.

Anisotropic electronic structure modification under strain has profound consequences. Since uniaxial strain acts as a field conjugate to the nematic order param-

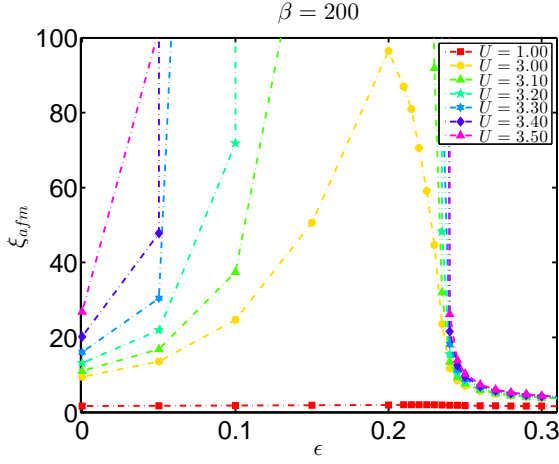


FIG. 3. Antiferromagnetic correlation length  $\xi_{afm}$  plotted as a function of strain  $\epsilon$  for various values of interaction, at  $\beta = 200$ . Antiferromagnetic fluctuations rapidly become critical with increasing  $U$  as seen from the figure.

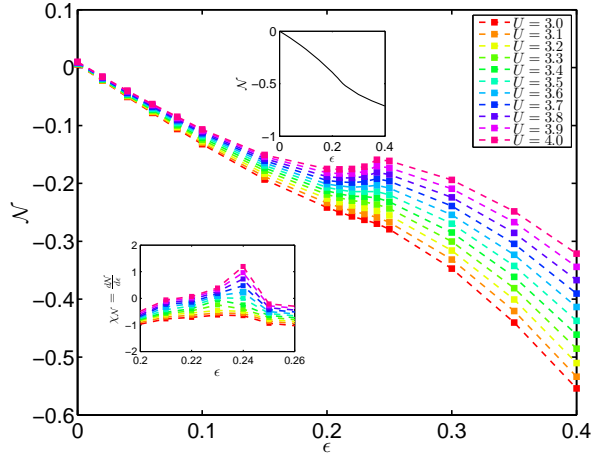


FIG. 4.  $\mathcal{N} = \frac{\langle\langle T_{xx} - T_{zz} \rangle\rangle}{\langle\langle T_{xx} + T_{zz} \rangle\rangle}$ , plotted as a function of strain  $\epsilon$  for given values of interaction. The upper inset shows  $\mathcal{N}$  for  $U = 0$ . The lower inset shows the nematic susceptibility,  $\chi_N = \frac{d\mathcal{N}}{d\epsilon}$ , which shows singular behavior around critical strain due to interplay between anisotropic band structure and critical AFSF.

eter, electronic nematic (EN) criticality itself will be washed out by strain, ruling out EN itself as a candidate for the quantum phase transition (QPT) under strain. However, since strong AFSF directly feed back on the TPSC self-energy<sup>11</sup> and hence the renormalized propagator, the non-trivial renormalization effects do show up in  $G(\mathbf{k}, i\omega_n) = [G_0^{-1}(\mathbf{k}, i\omega_n) - \Sigma(\mathbf{k}, i\omega_n)]^{-1}$ . Computing the average (renormalized) kinetic energies along  $xx, zz$  bonds from  $G(\mathbf{k}, i\omega_n)$  thus allows for a direct estimate of the influence of strong AFSF in enhancing strain-induced electronic anisotropy, and hence on *bond* EN state. In Fig. 4, we show variation of  $\mathcal{N} = \frac{\langle\langle T_{xx} - T_{zz} \rangle\rangle}{\langle\langle T_{xx} + T_{zz} \rangle\rangle}$ , with  $\langle T_{\mu\mu} \rangle = \langle c_{i\sigma}^\dagger c_{i+\mu, \sigma} \rangle$  with  $\mu = x, z$  without and with

the Hubbard  $U$ . It is rather clear that EN “order” is significantly enhanced by strong AFSF, the origin of which is anisotropic suppression of  $\langle T_{xx} \rangle$  relative to  $\langle T_{zz} \rangle$ , the latter itself being a direct consequence of AFSF-driven anisotropic renormalization of  $t_{x,x} < t_{z,z}$  under strain. Finally, notwithstanding the absence of quantum criticality associated with EN order, we find that  $d\langle N \rangle/d\epsilon$  shows an abrupt change precisely around  $U_c(\epsilon)$ . Thus, there is evidence for nematic criticality as a function of strain: to characterize it, we observe that (i) if bond EN order would exist without strain, it would break the discrete ( $C_{6v}$  for graphene) rotational symmetry of the crystal lattice, implying spontaneous breaking of an Ising-like symmetry, but (ii) strain washes out this criticality. However, since strain is a field conjugate to  $\langle N \rangle$ , nematic criticality can still occur<sup>16,17</sup> at finite strain, as in Fe arsenides. Such a criticality should show up as a divergent nematic susceptibility,  $\chi_N(\epsilon) = d\mathcal{N}/d\epsilon$ , near  $U_c$ . In the inset to Fig. 4, we show that this is indeed what we find. This leads us to the central conclusion of this work: *a nematic quantum criticality of the quantum liquid-gas variety, driven by strong AFSF around the critical  $U_c$ , underlies the “transition” from Dirac-LFL to an incoherent metal near critical strain.*

Lack of LFL quasiparticles for  $U > U_c(\epsilon)$  as above implies that one should expect an (anisotropic) breakdown of the Wiedemann-Franz (WF) law. This has recently been shown to occur for neutral graphene, leading to possibility of a novel “Dirac liquid”<sup>6</sup> with transport due to collective excitations. Thermal and electrical transport under strain could help in determining the fate of the WF law under strain. However, use of strain as a tuning parameter suggests that studying magnetic-fluctuation contributions to magneto-volume, thermal expansion and Grüneisen co-efficients could more naturally facilitate observation of the above QPT. That it is possible to reversibly tune the strain to about 20 percent could make the above scenario realistically possible. Motivated hereby, we now propose that critical divergences in thermal expansion and magnetic Grüneisen co-efficients due to divergent AFSF near  $\epsilon_c$  can be fruitfully employed to unearth the novel criticality proposed here.

In our picture, coupling of strain to AFSF results in a magneto-elastic interaction. This will have novel consequences for spin fluctuation contribution to the magneto-volume, defined as  $\omega_m(T) = \delta V(T)/V$  and thermal expansion co-efficient,  $\alpha_m(T) = \partial \omega_m / \partial T$ . Such effects have long been well-documented in  $d$ -band transition metals and compounds and explicated by the well-known Moriya-Usami approach<sup>18</sup> within SCR theory. Given that TPSC is an advanced variant of SCR theory, we can use the SCR formulation to investigate magneto-elastic effects in strained graphene.

Moriya-Usami theory asserts that electronic correlation or spin fluctuation contribution to the magneto-volume in the quantum paramagnetic state ( $T > T_N (= 0)$  in  $D = 2$ ) is related, apart from parameters  $D_0$  (re-

lated to the strain dependence of the band-width via  $D_0 = \frac{\partial \ln(W)}{\partial \ln \epsilon}$  and  $B$ , the bulk modulus, to the magnetic fluctuations,  $\langle \delta M^2 \rangle = (\langle S_z^2 \rangle)$ , the latter evaluated in the quantum paramagnetic phase. This can be evaluated using  $D = \langle n_\uparrow n_\downarrow \rangle = (n - \langle S_z^2 \rangle)/2$ , with  $D$ , the double occupancy evaluated from TPSC (from  $\chi(\mathbf{q}, i\omega_n)$ ) using the TPSC sum rule, providing a direct way to study magnetoelastic effects near the QCP above. In Fig.5, we show  $\omega_m(T)$  and  $\alpha_m(T)$  for a range of  $U$  near critical strain to illustrate the main features of interest.  $D_0$  is negative and of the order of 1, while  $B \approx 200 \text{ Nm}^{-1}$ .

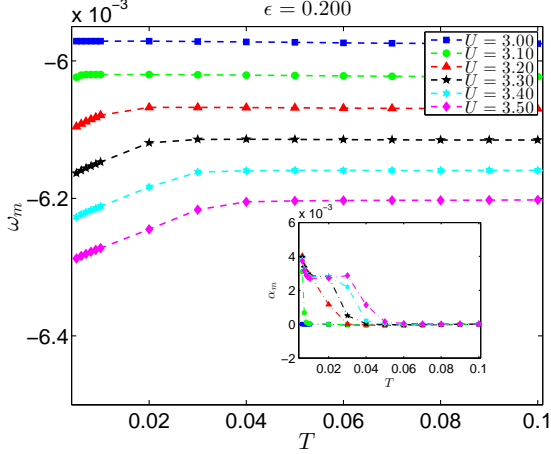


FIG. 5. Magneto-volume,  $\omega_m$  as a function of temperature  $T$ . The inset shows a plot of thermal expansion co-efficient,  $\alpha_m$  as a function of  $T$ , showing how it diverges as  $T \rightarrow 0$  due to coupling of strain to critical AFSF for  $U \geq 3.2$  near critical strain ( $\epsilon = 0.20$ ).

Interestingly, though the magnetic fluctuation contribution to  $\omega_m(T), \alpha_m(T)$  is sizable at small strain, we find that *both* contributions vanish as  $T \rightarrow 0$ . Beyond a strain-dependent  $U_c(\epsilon)$ , however, marked changes show up: most interestingly, the influence of long-range critical AFSF reveal themselves in a critical divergence in  $\alpha_m(T \rightarrow 0)$ . Further, this should have direct bearing on the divergence of the *magnetic* Grüneisen co-efficient, defined as  $\Gamma_m(T) = \alpha_m(T)/C_{el}(T)$ , where  $C_{el}(T)$  is the electronic contribution to the specific heat. It is numerically involved to compute  $C_{el}$  within TPSC: however, we expect  $C_{el}(T) \simeq T^2$  in  $D = 2$  up to logarithmic corrections (in fact, within the field-theoretic RG work of Sheehy *et al*<sup>10</sup>, one finds  $C_{el}(T) \simeq T^2/(1 + b \log T)^2$  with  $b$  a constant. If this were to qualitatively hold right up to  $U_c, \epsilon_c$  from the LFL side, it would imply that  $\Gamma_m(T \rightarrow 0)$  would also show a critical divergence. Furthermore, these hallmarks of quantum criticality disappear beyond critical strain<sup>8</sup>, pinning them to the influence of critical AFSF.

Anomalies in  $\omega_m(T), \alpha_m(T)$  and  $\Gamma_m(T)$  have recently received intense attention in the context of quantum criticality in *d*- and *f*-band materials<sup>19</sup>. We can now rationalize the critical divergence of  $\alpha_m, \Gamma_m$  near critical

strain at  $U$  close to  $U_c(\epsilon)$ . These are directly related to singular  $T$ -dependence of  $\partial \langle S_z^2 \rangle / \partial T$  due to diverging AFSF at sizable  $U$  in the vicinity of  $\epsilon_c$  as shown above. In light of inducement of reversible strain<sup>5</sup> up to 20 percent, such a novel QCP with diverging nematic susceptibility at finite strain is potentially realizable in practice. More generally, *metallic* honeycomb materials involving *Cu* in  $d^9$  configuration<sup>20</sup> (whence modelled by one-band Hubbard model) could exhibit such anomalies as we find near a pressure-driven Mott transition between a spin-liquid insulator and (incoherent) metal. We con-

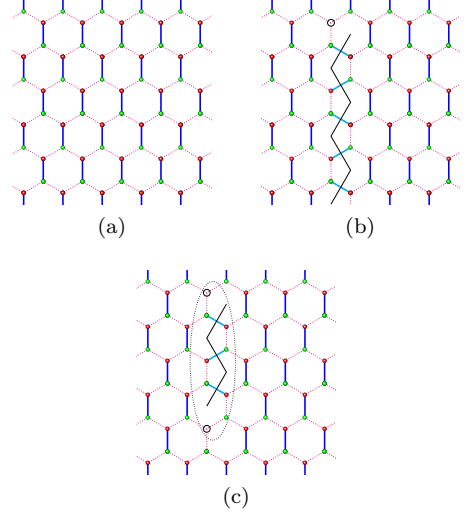


FIG. 6. Combination of anisotropic strain and strong AFSF beyond  $\epsilon_c$  produces a valence bond solid correlated insulator (panel (a)), with preferential dimerization of  $z-z$  bonds of the honeycomb lattice. A single doped hole (panel (b)) generates a “defect string” of singlets with local Kekule like structure, inhibiting coherent one-hole propagation. With two doped holes (panel (c)), the defect string of singlets is healed. This allows the hole pair, along with the intervening three singlets (shown as the dashed loop in panel (c)), to propagate coherently through the lattice.

clude by discussing the novel prospect of fractionalization of added electrons (holes) in heavily strained graphene. Since  $t_{x,x} < t_{z,z}$  is enhanced by AFSF under strain, it is reasonable to expect that at sizable  $U > U_c$  *i.e.*, in the correlated “band” insulator beyond  $\epsilon_c$ , the combined effect will be to readily promote spin-singlet valence-bond pairing on  $zz$ -bonds. As shown in Fig. 6, it then follows that this state can be viewed as a  $D = 2$  generalization of (dimerized) polyacetylene. In our case, it is the interplay between strain and strong AFSF (which also promotes the nematic state) which produces the dimerized state in the insulator. In the spinful case of relevance here, a single doped hole corresponds to a missing state in the valence band, and unoccupied, singly and doubly occupied states correspond<sup>21</sup> to charge and spin quantum numbers ( $Q = -e, S = 0$ ), ( $Q = 0, S = 1/2$ ) and ( $Q = e, S = 0$ ). In panel (b) of Fig. 6, we schematically show how a doped hole results in generation of an extended “string defect”

of singlets emanating from the bond hosting the hole: clearly the unpaired spin, originally in the vicinity of the hole, separates from it by creating such a string. Thus, a doped hole will fractionalize into a spinless *holon* and a spin-1/2 spinon! In the continuum limit, this could be seen by solving the Bogoliubov-de Gennes like equation for a doped hole, which results in only *one* renormalizable solution for a vortex or antivortex. This bares an alternative route to create fractionalized excitations by strain tuning in honeycomb lattice models. These solitonic excitations are defects in the dimerized ground state, and have exciting consequences. Specifically, beginning with such an insulator, doping should lead to a fractionalized state, wherein electrical current is carried by holons but the Hall current by spinons, as is implicit in the two-relaxation rate scenario<sup>22</sup>. Further, if two doped holes sit on different dimers, the hole pair, dressed by the dynamically fluctuating short-range singlet correlations (see the

dashed region in Fig. 6, panel (c)) could hop as a composite pair without scrambling the background spin configuration, leading to unconventional superconductivity in a spin-gapped background (this would be a  $D = 2$  version of the Luther-Emery scenario in  $D = 1$ ). Our study points toward such exotic possibilities, but we leave more detailed exploration of these themes for the future.

To conclude, we have presented a specific scenario to realize a range of unconventional states of matter by use of “clean” strain-tuning in graphene. Our work motivates study of other interesting materials like phosphorene, silicene, among other honeycomb systems, whose unstrained structures bear some resemblance to graphene. It should also be an attractive tool to investigate novel strain-induced QPTs in topological and Weyl systems, where the role of sizable Coulomb interactions remains largely unexplored, and should be a theme of potential interest.

---

\* aryas@imsc.res.in

† mslaad@imsc.res.in

‡ shassan@imsc.res.in

<sup>1</sup> A. H. Castro Neto, F. Guinea, N. M. R. Peres, K. S. Novoselov, and A. K. Geim, *Rev. Mod. Phys.* **81**, 109 (2009).

<sup>2</sup> F. Liu, P. Ming, and J. Li, *Phys. Rev. B* **76**, 064120 (2007).

<sup>3</sup> A. K. Geim and K. S. Novoselov, *Nat Mater* **6**, 183 (2007).

<sup>4</sup> V. M. Pereira, A. H. Castro Neto, and N. M. R. Peres, *Phys. Rev. B* **80**, 045401 (2009).

<sup>5</sup> Z. H. Ni, T. Yu, Y. H. Lu, Y. Y. Wang, Y. P. Feng, and Z. X. Shen, *ACS Nano* **2**, 2301 (2008), pMID: 19206396, <http://dx.doi.org/10.1021/nn800459e>.

<sup>6</sup> J. Crossno, J. K. Shi, K. Wang, X. Liu, A. Harzheim, A. Lucas, S. Sachdev, P. Kim, T. Taniguchi, K. Watanabe, T. A. Ohki, and K. C. Fong, *Science* **351**, 1058 (2016), <http://science.sciencemag.org/content/351/6277/1058.full.pdf>.

<sup>7</sup> L. Craco, S. S. Carara, and S. Leoni, *Phys. Rev. B* **94**, 165168 (2016).

<sup>8</sup> “See Supplementary information for (i) tight binding analysis of graphene under zig-zag strain, Sec (I), (ii) TPSC method and formalism for graphene under uniaxial strain, Sec (II A), (iii) TPSC as applied to graphene under strain, Sec (II B), (iv) more results for strain less than critical strain Sec (II C) and (v) scenario beyond critical strain, Sec. (III).”

<sup>9</sup> T. O. Wehling, E. Şaşıoğlu, C. Friedrich, A. I. Lichtenstein, M. I. Katsnelson, and S. Blügel, *Phys. Rev. Lett.* **106**, 236805 (2011).

<sup>10</sup> D. E. Sheehy and J. Schmalian, *Phys. Rev. Lett.* **99**, 226803 (2007).

<sup>11</sup> A. M. S. Tremblay, “Two-particle-self-consistent approach for the hubbard model,” in *Theoretical Methods for Strongly Correlated Systems*, Springer Series in Solid-State Sciences, Vol. 171, Vol. Springer Series, edited by F. Mancini and A. Avella (2011) Chap. 13.

<sup>12</sup> T. Moriya, *Spin fluctuations in itinerant electron magnetism*, Vol. 56 (Springer Science & Business Media, 2012).

<sup>13</sup> S. Chakravarty, B. I. Halperin, and D. R. Nelson, *Phys. Rev. B* **39**, 2344 (1989).

<sup>14</sup> D. Ogura and K. Kuroki, *Phys. Rev. B* **92**, 144511 (2015).

<sup>15</sup> A.-M. Daré, L. Raymond, G. Albinet, and A.-M. S. Tremblay, *Phys. Rev. B* **76**, 064402 (2007).

<sup>16</sup> J.-H. Chu, J. G. Analytis, K. De Greve, P. L. McMahon, Z. Islam, Y. Yamamoto, and I. R. Fisher, *Science* **329**, 824 (2010), <http://science.sciencemag.org/content/329/5993/824.full.pdf>.

<sup>17</sup> S. Kasahara, H. J. Shi, K. Hashimoto, S. Tonegawa, Y. Mizukami, T. Shibauchi, K. Sugimoto, T. Fukuda, T. Terashima, A. H. Nevidomskyy, and Y. Matsuda, *Nature* **486**, 382 (2012).

<sup>18</sup> T. Moriya and K. Usami, *Solid State Communications* **34**, 95 (1980).

<sup>19</sup> P. Gegenwart, Q. Si, and F. Steglich, *Nat Phys* **4**, 186 (2008).

<sup>20</sup> B. Zhang, Y. Zhang, Z. Wang, D. Wang, P. J. Baker, F. L. Pratt, and D. Zhu, *Scientific Reports* **4**, 6451 EP (2014), article.

<sup>21</sup> C.-Y. Hou, C. Chamon, and C. Mudry, *Phys. Rev. Lett.* **98**, 186809 (2007).

<sup>22</sup> P. W. Anderson, *Phys. Rev. Lett.* **67**, 2092 (1991).



# Supplementary Information for ‘Exploring Novel Quantum Criticality in Strained Graphene’

## I. TIGHT-BINDING ANALYSIS OF GRAPHENE UNDER STRAIN

The application of uniaxial strain on graphene has been studied in the tight-binding approximation by Pereira and co-workers<sup>S1</sup>. The major results are i) the application of strain opens up a gap in the bandstructure ii) the strain has to cross a threshold value for the gap to open up and iii) the application of strain along every direction does not result in a bandgap, for instance a strain along the armchair direction never opens a gap. Along the zigzag direction, a threshold strain of  $\epsilon_c > 0.23$  is needed for the gap to open up.

Figs. S1 and S2 show plots of the bandstructure and the density of states (DOS) corresponding to various values of strain along the zigzag direction. The plots in Fig. S1 are for strain values less than the critical strain required to open a bandgap, whereas in Fig. S2 the strain is larger than the critical strain.

## II. TWO-PARTICLE SELF-CONSISTENT METHOD FOR THE HUBBARD MODEL ON THE HONEYCOMB LATTICE UNDER UNIAXIAL STRAIN

As mentioned in the main text, in order to study the Hubbard model on the honeycomb lattice under uniaxial strain, the method we choose is the two-particle self-consistent approach (TPSC). This nonperturbative, semi-analytical technique is valid from weak to intermediate values of interaction. Initially developed as an approximation scheme to study the single-band Hubbard model on the square lattice<sup>S2,S3</sup>, TPSC was later extended to study the multi-band case of the Hubbard model<sup>S4-S6</sup>. In particular, the semi-metal to antiferromagnet transition of the half-filled Hubbard model on the honeycomb lattice was studied using this method<sup>S6</sup>.

TPSC satisfies many important physical constraints like conservation laws, Pauli principle and local sum rules for spin and charge susceptibilities. Most importantly, this approach obeys the Mermin-Wagner theorem, which prevents a finite temperature phase transition in two dimensions, while aptly capturing the physics of long wavelength antiferromagnetic fluctuations in the system. Once the antiferromagnetic correlation length becomes larger than the thermal de Broglie wavelength, there is a crossover to the renormalized classical regime. Since the quasiparticles get destroyed by these large antiferromagnetic fluctuations, a pseudogap opens up<sup>S2,S3</sup>.

### A. Method and Formalism

In TPSC, we start with the noninteracting susceptibility and define Bethe-Salpeter equations for the interacting spin and charge susceptibilities. Although TPSC looks similar to RPA, the irreducible vertices for the spin and charge channels are different, and are different from the bare interaction<sup>S2,S3</sup>. In the case of the honeycomb lattice, for our purposes we have a non-interacting susceptibility which is a  $2 \times 2$  matrix,

$$\chi_0(q) = \begin{bmatrix} \chi_0^{aaaa}(q) & \chi_0^{aabb}(q) \\ \chi_0^{bbaa}(q) & \chi_0^{bbbb}(q) \end{bmatrix} \quad (S1)$$

where  $q \rightarrow (\mathbf{q}, i\nu_n)$ ,  $\mathbf{q}$  is the momentum and  $i\nu_n$  is the bosonic Matsubara frequency. An element of the noninteracting susceptibility in the momentum-imaginary frequency representation is given by,

$$\chi_0^{\rho\lambda\lambda}(q) = -\frac{T}{N^2} \sum_{k\sigma} G_\sigma^{(0)\lambda\rho}(k) G_\sigma^{(0)\rho\lambda}(k+q) \quad (S2)$$

where  $\rho, \lambda = a, b$  are the sublattice indices on the honeycomb lattice and the lattice / momentum grid is of size  $N \times N$ . Here  $k \rightarrow (\mathbf{k}, i\omega_n)$ ,  $\mathbf{k}$  is the momentum and  $i\omega_n$  is the fermionic Matsubara frequency.

The spin and charge susceptibilities in the position-imaginary time representation are,

$$\chi_{sp}^{\rho\lambda\lambda}(1,2) = \langle T_\tau S_\rho^z(1) S_\lambda^z(2) \rangle \quad (S3)$$

$$\chi_{ch}^{\rho\lambda\lambda}(1,2) = \langle T_\tau n_\rho(1) n_\lambda(2) \rangle - \langle n_\rho \rangle \langle n_\lambda \rangle \quad (S4)$$

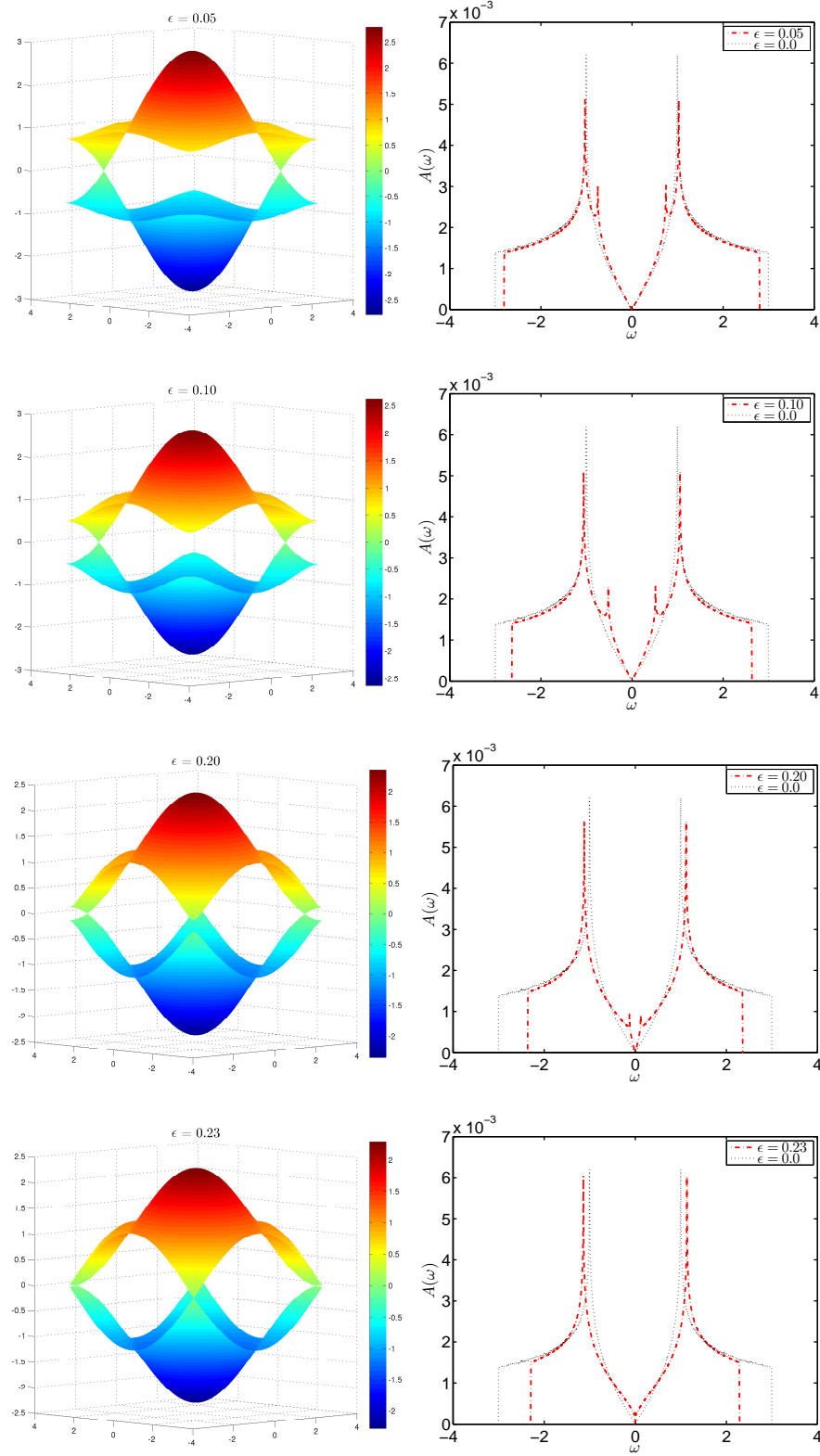


FIG. S1. Plots of bandstructure and density of states (DOS)  $A(\omega)$  for graphene under strain  $\epsilon$  along the zigzag direction. The values of strain shown here are less than the critical strain needed to induce a bandgap. The DOS for the unstrained case is also plotted in black dotted lines for comparison.

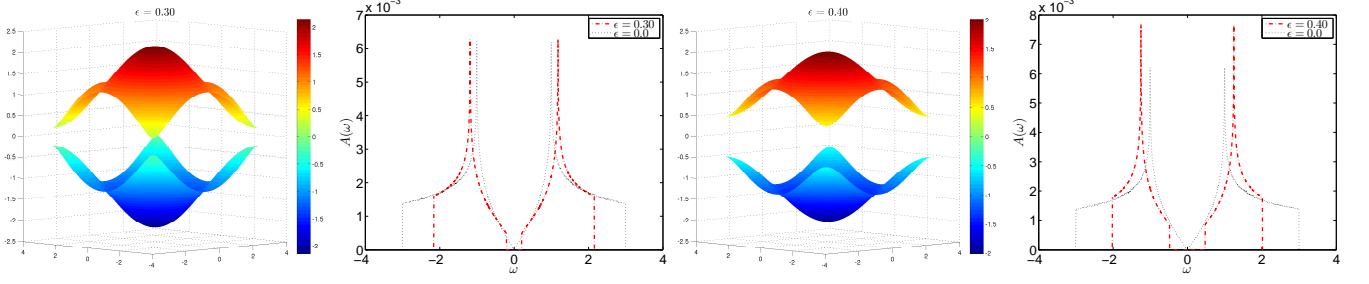


FIG. S2. Plots of bandstructure and density of states (DOS)  $A(\omega)$  for graphene under strain  $\epsilon$  along the zigzag direction. The values of strain shown here are greater than the critical strain. The gap is clearly visible in both the bandstructure and DOS plots.

Here 1 is a shorthand for  $(\mathbf{r}_1, \tau_1)$  the position and the imaginary time. From Eq.s (S3) and (S4), the local spin and charge sum rules are obtained when we set  $1 \rightarrow 2, \lambda = \rho$ ,

$$\frac{T}{N^2} \sum_q \chi_{sp}^{\rho\rho\rho\rho}(q) = \langle n_{\rho\uparrow} \rangle + \langle n_{\rho\downarrow} \rangle - 2\langle n_{\rho\uparrow} n_{\rho\downarrow} \rangle \quad (S5)$$

$$\frac{T}{N^2} \sum_q \chi_{ch}^{\rho\rho\rho\rho}(q) = \langle n_{\rho\uparrow} \rangle + \langle n_{\rho\downarrow} \rangle + 2\langle n_{\rho\uparrow} n_{\rho\downarrow} \rangle - n_\rho^2 \quad (S6)$$

The interacting spin and charge susceptibilities are given by

$$\chi_{sp}(q) = \left[ \mathbf{1} - \frac{1}{2} \chi_0(q) \mathbf{U}_{sp} \right]^{-1} \chi_0(q) \quad (S7)$$

$$\chi_{ch}(q) = \left[ \mathbf{1} + \frac{1}{2} \chi_0(q) \mathbf{U}_{ch} \right]^{-1} \chi_0(q) \quad (S8)$$

in terms of the noninteracting susceptibility. This is the matrix version of the scalar equation appearing in the single-band case<sup>S2,S3,S6</sup>. The elements of the matrix spin ( $\mathbf{U}_{sp}$ ) and charge ( $\mathbf{U}_{ch}$ ) vertices appearing in the above expression can be obtained as functional derivatives of the elements of the self-energy matrix with respect to the elements of the Green function matrix.

Using the TPSC ansatz, we can write a first approximation to the self-energy which is momentum and frequency independent<sup>S2,S3,S6</sup> and from this form of the self-energy we get a local spin vertex where the diagonal  $aaaa$  and  $bbbb$  elements are non-zero. This local spin vertex is given by

$$U_{sp} = U \frac{\langle n_{\uparrow} n_{\downarrow} \rangle}{\langle n_{\uparrow} \rangle \langle n_{\downarrow} \rangle} \quad (S9)$$

Because of sublattice symmetry  $\langle n_{a\uparrow} n_{a\downarrow} \rangle = \langle n_{b\uparrow} n_{b\downarrow} \rangle$  and  $\langle n_{a\sigma} \rangle = \langle n_{b\sigma} \rangle$ . Although the charge vertex is not local, and involves higher order correlation functions which are hard to compute, we assume that the charge vertex is also local ( $U_{ch}$ ).

We define ferromagnetic and the antiferromagnetic spin susceptibilities for both noninteracting and interacting cases as,

$$\chi_{0,sp}^{fm} = \chi_{0,sp}^{aaaa} - \sqrt{\chi_{0,sp}^{aabb} \chi_{0,sp}^{aabb}} \quad (S10)$$

$$\chi_{0,sp}^{afm} = \chi_{0,sp}^{aaaa} + \sqrt{\chi_{0,sp}^{aabb} \chi_{0,sp}^{aabb}} \quad (S11)$$

The interacting susceptibilities are related to the noninteracting ones by the relation

$$\chi_{afm,fm}^s = \frac{\chi_0^{afm,fm}}{1 - \frac{U_{sp}}{2} \chi_0^{afm,fm}} \quad (S12)$$

that resembles the scalar Bethe-Salpeter equations in the single-band case.



Focusing only on antiferromagnetic correlations, the correlation length  $\xi_{afm}$  can be quantified in terms of the ratio of the maximum of the interacting antiferromagnetic susceptibility to the maximum of the noninteracting antiferromagnetic susceptibility at  $(\mathbf{q} = 0, i\nu_n = 0)$ .

$$\xi_{afm} = \frac{\chi_{afm}^s(\mathbf{q} = 0, i\nu_n = 0)}{\chi_{afm}^0(\mathbf{q} = 0, i\nu_n = 0)} \quad (\text{S13})$$

$$(\text{S14})$$

The second approximation to self-energy including the effects of spin and charge fluctuations can be made as

$$\Sigma_\sigma(k) = Un_{\rho,-\sigma} + \frac{U}{4} \frac{T}{N^2} \sum G_\sigma^{aa}(k+q) [U_{sp}\chi_{sp}^{aaaa}(q) + U_{ch}\chi_{ch}^{aaaa}(q)] \quad (\text{S15})$$

We work at half-filling, and start by finding the noninteracting susceptibility  $\chi_0(q)$  using a combination of FFT and cubic splines for a momentum grid  $N \times N$  for  $N_\nu$  number of Matsubara frequencies. For a particular value of interaction  $U$ , a guess value of double occupancy  $\langle n_\uparrow n_\downarrow \rangle$  is chosen. Using the TPSC ansatz (S9) and the spin sum rule (S5), the double occupancy, and thereby the spin vertex ( $U_{sp}$ ) can be determined self-consistently. Once the double occupancy is obtained, using the charge sum rule (S6), we can solve for the charge vertex ( $U_{ch}$ ). Again by using a combination of FFTs and cubic splines we can compute the self-energy using (S15).

## B. Graphene under strain

The application of strain to the honeycomb lattice changes bond lengths. This results in a change in the reciprocal lattice vectors as well as a change in the hopping parameters. In our calculations, we assume the reciprocal lattice remains the same as the one corresponding to the undistorted lattice. We take into account only the change in the hopping parameters. In the case of unstrained graphene, the hopping parameters along all the three bonds are equal. Upon the application of strain, the hopping parameters are no longer isotropic. When a strain is applied along the zigzag direction, then  $t_{x,x} = t_{y,y} < t_{z,z}$ . This in turn changes the dispersion relation. When we evaluate the noninteracting Green functions and the noninteracting susceptibilities, this information is taken into account. The rest of the procedure remains intact as mentioned in the previous section.

## C. Results

The results for double occupancy  $\langle n_\uparrow n_\downarrow \rangle$ , irreducible spin and charge vertices  $U_{sp}$  and  $U_{ch}$  and antiferromagnetic correlation length ( $\xi_{afm}$ ) for  $T = 0.01$  are shown in Fig. S3. These quantities have been plotted as functions of strain  $\epsilon$  for various values of  $U$ . As we can see, the antiferromagnetic fluctuations grow in magnitude with increasing interaction, at low values of temperature.

The imaginary part of self-energy as a function of the fermionic Matsubara frequency  $\omega_n$  has been plotted for various values of strain less than the critical strain. As mentioned in the main text, for no strain or very low strain ( $\epsilon = 0.05$ ), the Dirac Landau Fermi liquid remains stable till  $U = 3.5$ , whereas for  $0.1 \leq \epsilon \leq 0.23$ , for  $U > U_c(\epsilon)$ , the imaginary part of self-energy shows anomalous behavior. All these details can be seen from the plots in Fig. S4.

The spin fluctuation contribution to the magneto-volume was discussed in the main text. From the self-consistent value of double occupancy obtained, we can calculate  $\langle S_z^2 \rangle = 1 - 2\langle n_\uparrow n_\downarrow \rangle$ . The plots of this quantity as a function of temperature for various values of strain are given in S5. As temperature decreases, the antiferromagnetic fluctuations in the system become large and  $\langle S_z^2 \rangle$  also increases as a consequence.

Similarly, the derivative of  $\langle S_z^2 \rangle$  with respect to temperature  $T$  ( $\frac{d\langle S_z^2 \rangle}{dT}$ ) is plotted in Fig. S6 for various values of strain. For  $T \rightarrow 0$ , for  $0.1 < \epsilon \leq 0.23$ , the derivative tends to diverge beyond  $U > U_c(\epsilon)$ . This, as previously stated in the main text refer to quantum criticality associated with large antiferromagnetic fluctuations.

This can be further substantiated by plotting the derivative of  $\langle S_z^2 \rangle$  with respect to strain  $\epsilon$  ( $\frac{d\langle S_z^2 \rangle}{d\epsilon}$ ), as a function of strain for various values of temperature as shown in Fig. S7. For low values of temperature, beyond  $U > U_c(\epsilon)$ , the singularity in the derivative points to the existence of a phase transition driven by the growing antiferromagnetic fluctuations.

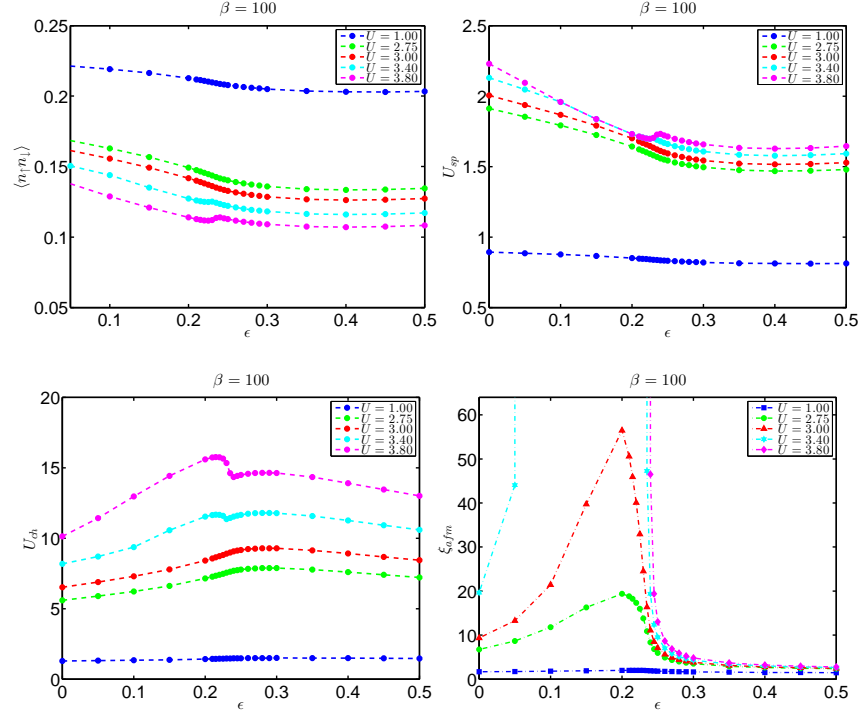


FIG. S3. Plots of double occupancy ( $\langle n_{\uparrow}n_{\downarrow} \rangle$ ), irreducible vertices ( $U_{sp}$ ,  $U_{ch}$ ) and antiferromagnetic correlation length  $\xi_{afm}$  as functions of strain  $\epsilon$  at  $\beta = 100$ . Interaction values ( $U$ ) are indicated in the legend.

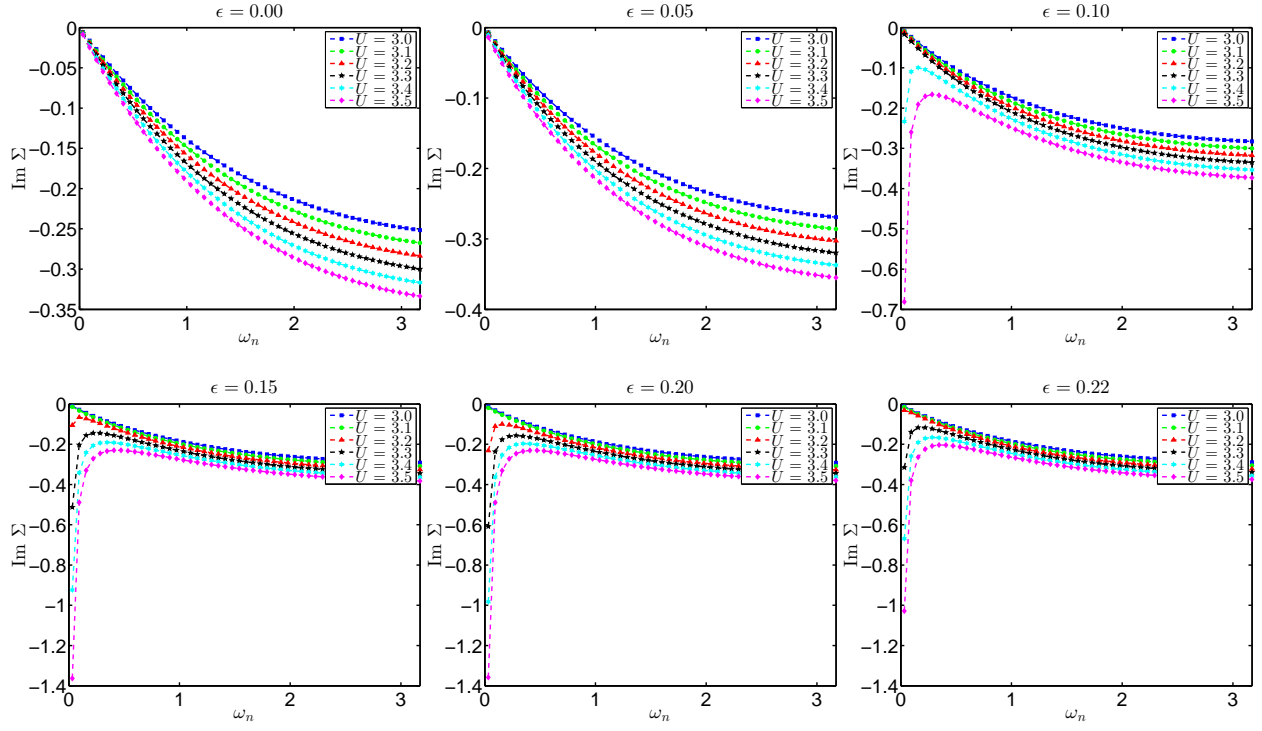


FIG. S4. Imaginary part of the self energy  $\Sigma$  plotted as a function of Matsubara frequency  $\omega_n$ , for various values of strain  $0.0 \leq \epsilon < 0.23$  for  $\beta = 100$ . The legend indicates the values of interaction  $U$ .

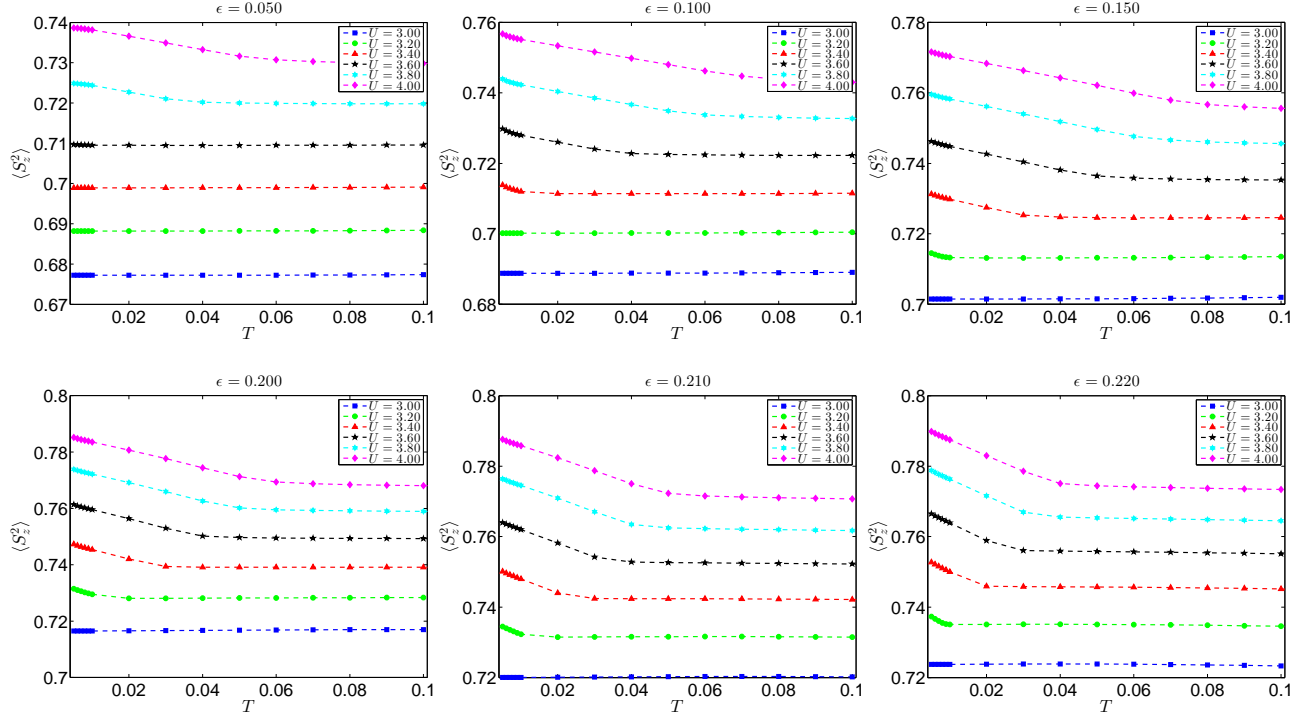


FIG. S5. Plots of  $\langle S_z^2 \rangle = 1 - 2\langle n_\uparrow n_\downarrow \rangle$  as a function of temperature  $T$ , for various values of strain  $\epsilon$  below the critical strain. The legends indicate the values of interaction  $U$ .

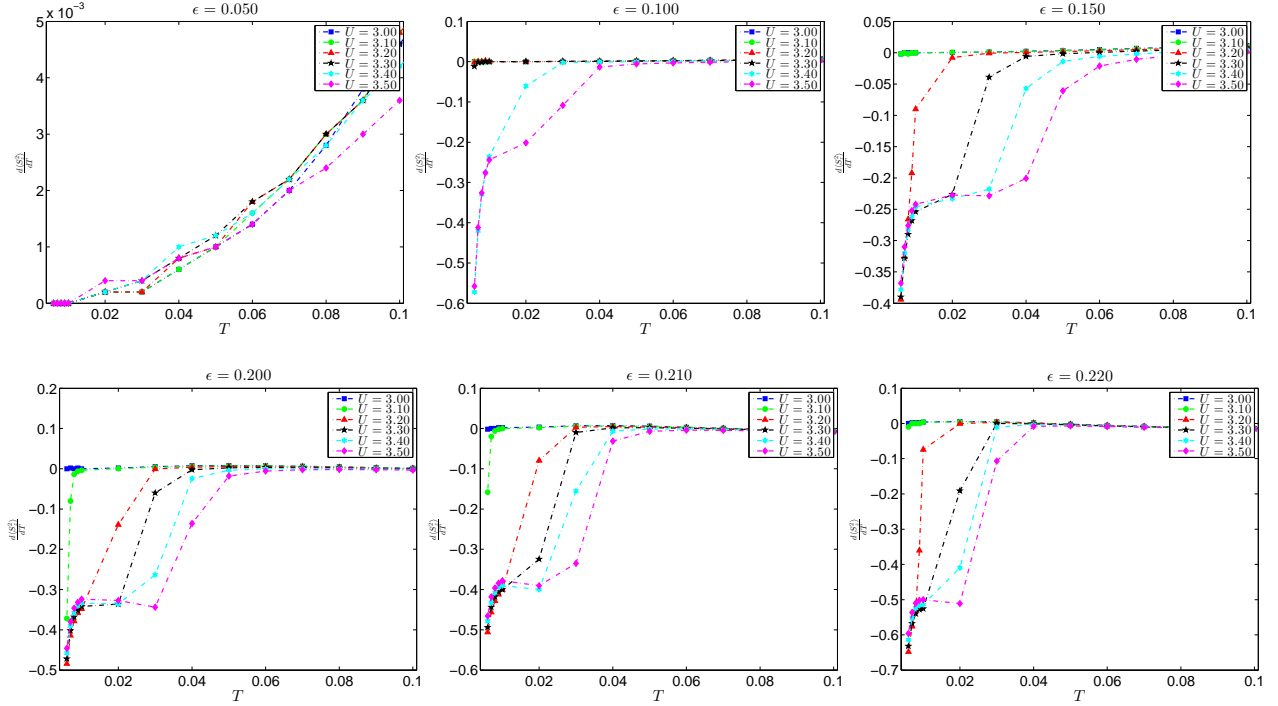


FIG. S6. Plots of  $\frac{d\langle S_z^2 \rangle}{dT}$  as a function of temperature  $T$ , for various values of strain  $\epsilon$  below the critical strain. The legend indicates the values of interaction  $U$ .

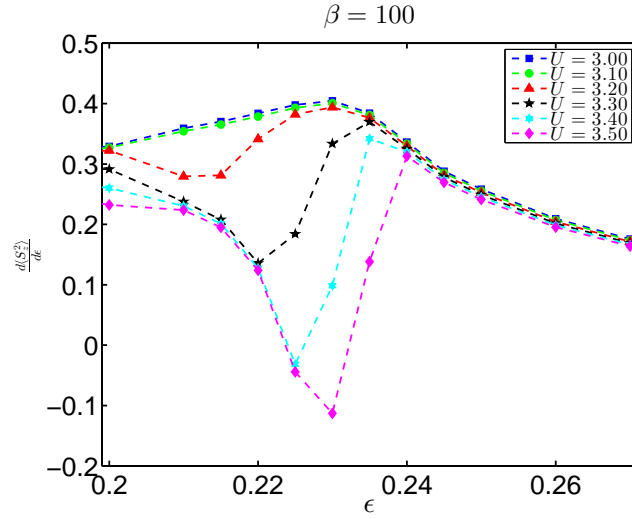


FIG. S7. Plots of  $\frac{d\langle S_z^2 \rangle}{d\epsilon}$  as a function of strain  $\epsilon$ , for  $\beta = 100$ . The values of interaction  $U$  are given in the legend.

### III. SCENARIO BEYOND CRITICAL STRAIN

For values of strain beyond the critical strain  $\epsilon \geq 0.24$ , the system becomes a band insulator. The main result is that even at low temperatures, the antiferromagnetic fluctuations do not become huge as seen from the plots in Fig. S8. These corroborate the statement in the main text that the features of quantum criticality are influenced by the growing antiferromagnetic fluctuations in the system. Since the antiferromagnetic fluctuations do not become huge,

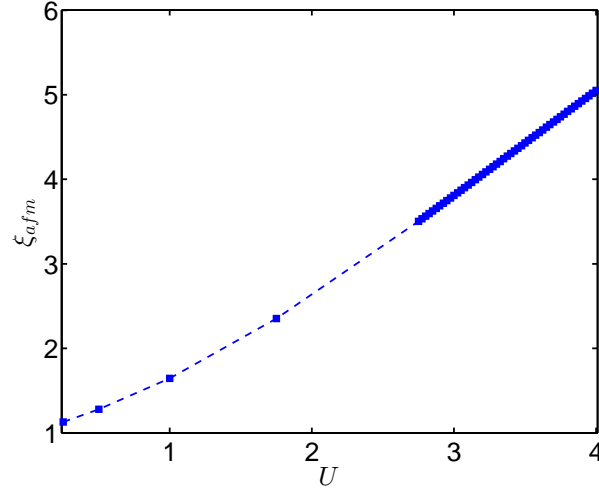


FIG. S8. Plot of antiferromagnetic correlation length ( $\xi_{afm}$ ) for  $\epsilon = 0.3$ , at  $\beta = 100$ . It can be clearly seen that the antiferromagnetic fluctuations do not grow large.

we do not expect the self energy to show any anomalous feature as  $\omega_n \rightarrow 0$ . This can be seen clearly from Fig. S9 where we have plotted imaginary part of the self-energy as a function of the fermionic Matsubara frequency, for values of strain beyond the critical strain. The plots of  $\langle S_z^2 \rangle$  in Fig. S10 and the derivative of  $\frac{d\langle S_z^2 \rangle}{dT}$  in Fig. S11 also give us the same information. From the plots of Fig. S10, we can see that  $\langle S_z^2 \rangle$  is almost temperature independent, for the same values of interaction at which we see large antiferromagnetic fluctuations in the system below critical strain. And,  $\frac{d\langle S_z^2 \rangle}{dT}$  does not diverge as  $T \rightarrow 0$ , and is almost independent of the value of interaction.

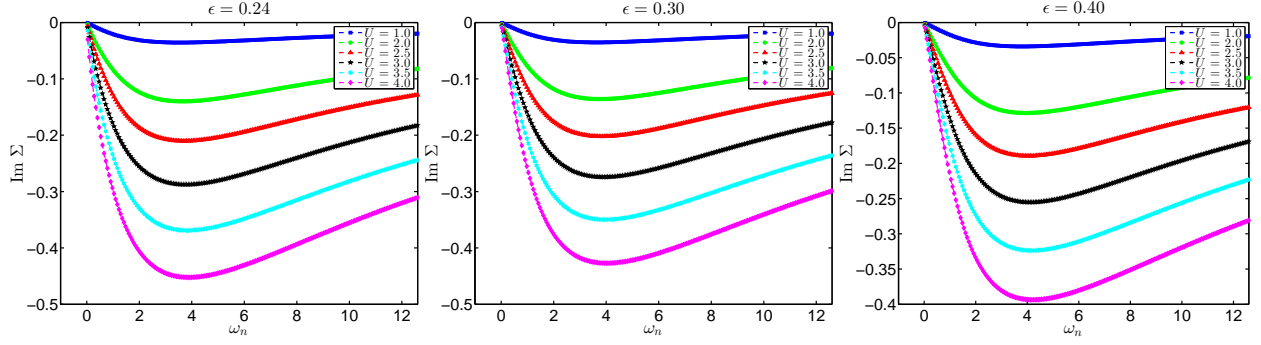


FIG. S9. Imaginary part of the self energy  $\Sigma$  plotted as a function of Matsubara frequency  $\omega_n$ , for various values of strain  $\epsilon$  greater than critical strain for  $\beta = 100$ . The values of interaction  $U$  are shown in the legend.

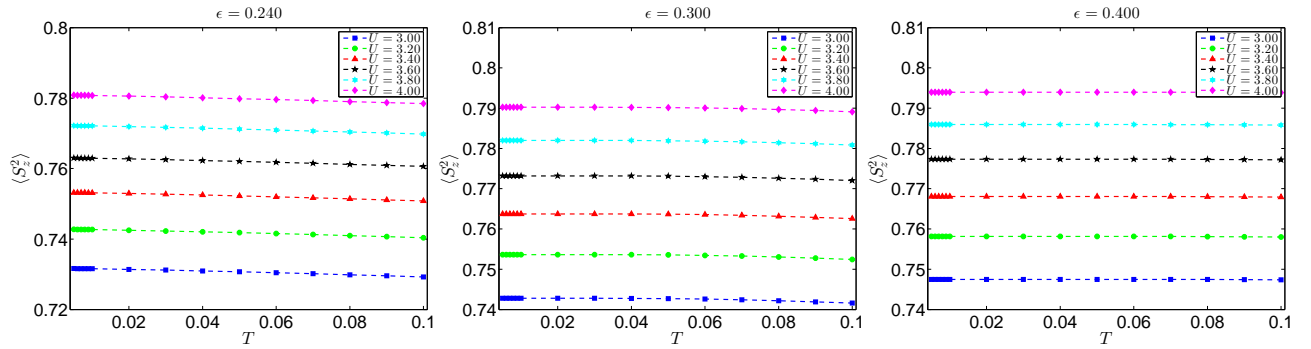


FIG. S10. Plots of  $\langle S_z^2 \rangle = 1 - 2\langle n_\uparrow n_\downarrow \rangle$  as a function of temperature  $T$ , for various values of strain  $\epsilon$  greater than the critical strain. The legend indicates the values of interaction  $U$ .

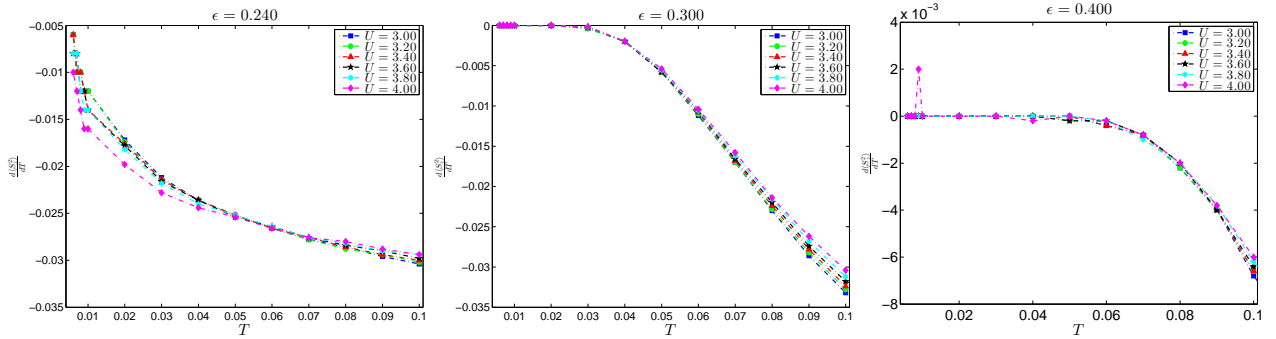


FIG. S11. Plots of  $\frac{d\langle S_z^2 \rangle}{dT}$  as a function of temperature  $T$ , for various values of strain  $\epsilon$  greater than the critical strain. The legend indicates the values of interaction  $U$ .

\* aryas@imsc.res.in

† msllaad@imsc.res.in

‡ shassan@imsc.res.in

[S1] V. M. Pereira, A. H. Castro Neto, and N. M. R. Peres, Phys. Rev. B **80**, 045401 (2009).

[S2] Y. Vilk and A.-M. Tremblay, Journal de Physique I **7**, 1309 (1997).

[S3] A.-M. S. Tremblay, in *Strongly Correlated Systems* (Springer, 2012) pp. 409–453.

[S4] H. Miyahara, R. Arita, and H. Ikeda, Phys. Rev. B **87**, 045113 (2013).

- [S5] D. Ogura and K. Kuroki, Phys. Rev. B **92**, 144511 (2015).
- [S6] S. Arya, P. V. Sriluckshmy, S. R. Hassan, and A.-M. S. Tremblay, Phys. Rev. B **92**, 045111 (2015).